Hindawi
Advances in Civil Engineering
Volume 2019, Article ID 2367635, 14 pages
https://doi.org/10.1155/2019/2367635

Research Article

Frost Heave of Irrigation Canals in Seasonal Frozen Regions

Jian Xu,[1] Qinze Wang,[2] Jiulong Ding,[2] Yanfeng Li,[1] Songhe Wang,[2] and Yugui Yang[3]

[1]*School of Civil Engineering, Xi'an University of Architecture and Technology, Xi'an, Shaanxi 710055, China*
[2]*Institute of Geotechnical Engineering, Xi'an University of Technology, Xi'an, Shaanxi 710048, China*
[3]*State Key Laboratory for Geomechanics and Deep Underground Engineering, China University of Mining and Technology, Xuzhou, Jiangsu 221008, China*

Correspondence should be addressed to Songhe Wang; wangsonghe@126.com

Received 16 July 2018; Revised 9 November 2018; Accepted 22 November 2018; Published 14 January 2019

Academic Editor: Robert Černý

Soil frost heave acts as a driver of the emerged fracture in the concrete lining of irrigation canals and subsequent water leakage in seasonal frozen ground. A model test was carried out on the frost heave of a U-shaped canal with concrete lining. The heat and water migration during freezing, and frost heave-induced deformation, and force in normal direction were live monitored by high-precision transducers. The results prove that the freezing front descends downward over time at a specified thermal boundary, with considerable migration of water within the scope of 0–40 cm. The maximum deformation occurred at the bottom of the lining and decreased upward with the rate of frost heave lowering over time while the normal force showing little change in the monitoring points, implying that stress concentration does not show up during freezing. Besides, the layered settlement observation reveals that frost heave dominates the total deformation while creep, the universal source of deformation, accounts for a negligible proportion. A practical model was proposed based on a simple theoretical model for heat-water coupled transfer in a partially saturated medium and was numerically implemented in COMSOL. The computed results were compared with the monitored data including frozen depth, water content, normal displacement, and frost heave force. Finally, the rational thickness of the insulation board was determined based on the partial insulation method.

1. Introduction

Water resource shortage is a great constraint for the development of economy and society in China, especially for the backbone of the country, viz., agriculture [1]. Irrigation canals with length exceeding three million kilometres are built in large irrigation areas. However, the lower proportion for canals with concrete lining has led to an alarming water leakage of about 173.4 bn·m^3 per year [2, 3]. Even more severe is the threatening frost damage of lining structure under seasonal frost actions [4], as presented in Figure 1. The embedded depth of foundation was generally set below the frozen depth to address this issue, and the work quantity devoted may occupy about one-third of the overall. This may be valid in constructing small-scale water conservancy projects; however, this kind of antifrost measure is impossible for a large irrigation area by simply increasing the burial depth in view of the large expense. Thus, a rational estimation of frost heave in irrigation canals is required to provide guidance for formulating more economic antifrost countermeasures [5].

Frost damage in irrigation canals primarily originates from the frost heave of foundation soils. Specifically, two physical processes are included such as water migration and ice segregation [6, 7]. For the former, the ice and water pressure and ice segregating temperature were combined by both capillary model and generalized Clausius–Clapeyron equation, and the changes in ice content, permeability, and deformation were incorporated in constructing frost heave theory [8, 9]. The ice content was indirectly obtained by the variation of unfrozen water content with temperature that can be easily determined by nuclear magnetic resonance (NMR), differential scanning clorimetry (DSC), and time-domain reflectometry (TDR) and can be empirically derived from simple functions [10]. However, one another point to be concerned even if ice

(a) (b)

Figure 1: Frost damage in irrigation canals. (a) Swelling of lining. (b) Dislocation.

movement can be neglected is what kind of driving force has induced water migration during soil freezing. The film water movement, ice segregating pressure, matric suction, and even the thermomolecular pressure are introduced to up-to-date works [11]. The migration of water is affected by various factors, e.g., thermal regime, initial water content, dry density, availability of external water, particle grading characteristics, and mineral composition [12]. Experiments prove that the freezing rate is directly proportional to the gradient of temperature and in situ water close to the freezing front rapidly freezes with a shorter duration to stabilize [12]. However, this may be prolonged at higher water contents in which more water participated in the ice-water phase change, as noted from soil freezing curves [13]. Provided that the occupied space of unfrozen water was compressed, e.g., larger compaction degree, the fierce phase transition may not be that easily perceived, whereas a certain amount of unfrozen water still exists at extremely low temperatures despite this [14]. The freezing front proceeds at a lower rate in the open freezing system while only part of the unfrozen water in soil mass moves towards the freezing front in closed freezing system [15]. Soils with the majority of particles exceeding 2 mm exhibits weak capillary force due to the better drainage performance, while for clayey soils that are mainly composed of finer particles, e.g., <0.005 mm, the strong absorption results in better water retention behavior and thereby the migration of water is quite weak. In this case, the clayey soil was classified as the frost susceptible soil [7, 16].

The main theme of the latter, i.e., ice segregation, is the cryotexture and characteristic parameters of the frozen fringe that acts as the necessary condition for ice lens formation. So far, high-tech methods such as X-ray radiography and charge-coupled device (CCD) are applied in locating the frozen fringe and cryotexture characters, e.g., the thickness can be ascertained [17, 18]; of course, the correlations with loading, rate of freezing, and ice segregating are included [12, 19]. The movement of water in frozen fringe is found to obey Darcy's law [20]. The hydraulic conductivity, the characteristic hydrodynamic index for frozen fringe, decreases with temperature, and the reduction of unfrozen water also played a considerable role [21, 22]. Another point to be concerned is the ice segregation criterion. It was in general given in the stress state, e.g., the separation pressure [23]. Azmatch et al. [6] defined a new concept of ice-entry value from the soil freezing curve based on the assumption that ice segregation results from the fracture of frozen fringe where newly formed ice lens intrude. In addition, Konrad [24] used the failure strain as the standard to justify whether the segregated ice was produced in frozen fringe. Style and Peppin [25] analyzed the growth rate of segregated ice in freezing porous media, and the commonly employed Clapeyron equation is not valid at the interface between the ice lens and the surrounding porous medium owing to the viscous dynamics of flow in premelted films for typical colloidal materials.

Empirical models that are easy to be used are based upon curve fitting of frost heave experiments [26], e.g., the modified Takashi model [27]. However, the complex migration of both heat and water and the ice segregation criterion cannot be well reflected by a single parameter, e.g., the discontinuous ice lens. The incorporation of the generalized Clausius–Clapeyron equation provides a possible solution to the above problems, and coupled migration of heat and water can be conveniently modeled [9], e.g., two of the most representative models such as the rigidice model and segregation potential model. The former is a relatively complete theoretical model that new ice lens is formed as the effective stress within the frost fringe could balance the overburden pressure. The nonlinear heat and mass transfer equation utilized here is merely applicable in frozen fringe but is flawed in too many undetermined parameters that lack physical significance and time-consuming computation required. Moreover, the thermodynamic model based on the balance of mass, momentum, energy, and entropy increase requires rational descriptions for both free energy and dissipated potential in constructing the porous medium model [28]. Based on the theories above, some antifrost measures are suggested in designing irrigation canals in seasonal frozen ground, such as avoiding construction sites with high ground water table, adjusting the lining structure to adapt to the potential frost heave or thaw settlement, and cutting down heat absorption in frozen ground by heat insulation, replacement, and drainage. Besides, the intermittent freezing mode [29] and partial insulation method [30] can also facilitate solving this problem.

To reveal the mechanism of frost heave in canal lining, this paper carries out a model test on a large U-shaped irrigation canal with concrete lining structure. The coupled heat and water migration and frost heave-induced deformation and force in the normal direction are investigated based on the monitored data. Then, based on the assumption of frost heave in soil originated from the phase transition of both migrated and original water into ice and in situ water into ice, a practical frost heave model is constructed with a simple equation for coupled heat and water migration. The model is numerically implemented in the COMSOL platform, and the rational thickness of the insulation board is discussed based on the partial insulation method.

2. Model Test on Frost Heave of a U-Shaped Irrigation Canal in Loess Stratum

2.1. Overview of the Jinghui Irrigation Area. A typical section selected from a branch canal in the Jinghui Irrigation Area is taken as the prototype in the model test. The gravity irrigation mode with water intake from the Jing River is used in about 9×10^4 hectares of farmland. This area is neighboring the loess tableland in the north while surrounded by Jing River, Wei River, and Shichuan River in the other three directions, with a length of 70 km from east to west and width of 20 km from south to north. The total area is about 1180 km^2, at an altitude ranging from 350 to 450 m. The climate for the Jinghui Irrigation Area is the typical continental semiarid region. The characteristic meteorological data obtained from the local meteorological stations are listed in Table 1. After years of maintenance and extension, five trunk canals with a total length of 80.6 km and nineteen branch canals with a length of 299.8 km are constructed. The designed discharge is 4.5 m^3/s for this canal with the lining structure produced by C20 cast-in-place concrete. The roughness and longitudinal slope for the lining structure are 0.015 and 1/1500, respectively. This canal is not put into service in winter, and the normal canal freeboard is 0.6 m. The arc-shaped open canals are mostly used, e.g., arc bottom trapezoid, arc angle trapezoid, and U-shaped canals, of which the U-shaped canal is frequently encountered in branches that are applicable to lower discharge cases. This type of section was developed in the Shaanxi province in 1970s. About 3.7% of the irrigated water will be saved compared with the trapezoid section, and this can reach 97% in comparison with the earth canal without lining. Besides, the merits also include better hydrodynamic capacity, antisedimentation, and smaller coverage area.

2.2. Model Design for a Typical Section along the Branch Canal. The loess samples were taken from a branch canal in Jingyang County, at a depth of 3–5 m. The basic physical parameters are listed in Table 2. The samples were crushed and sieved by a 2 mm geotechnical sieve. The distilled water was sprayed on the air-dried samples until the target water content was reached. The foundation of the canal model was prepared by layered compression of the prepared slurry, with the thickness of each layer not thicker than 20 cm. The canal cushion of nonwoven cloth geomembrane was set above the foundation soils with mortar leveling. The U-shaped lining board produced by C20 concrete was placed on the cushion. Besides, three layers surrounded the prepared canal model including geotechnical fabric, insulation board, and side wall, acting as barriers to the migration of heat and water transfer. The specific size for the prepared model was measured, and a deviation of lower than 2.0% was noted compared with the target size. The specific size for the irrigation canal is illustrated in Figure 2. Following the theory of similarity by Lai et al. [19], the similarity index can be written as

$$C_T \cdot C_t = C_l^2, \tag{1}$$

where C_t, C_l, and C_T are the similarity ratios of time, geometry, and temperature, respectively. Because the soil in the prototype was used in producing the canal model, and both water content and temperature are identical to the surveying site in situ. Thus, the effect of soil type on characteristic parameters can be neglected, i.e., elastic modulus, E; Poisson's ratio, v; heat conductivity, λ; water diffusivity, D; and latent heat, q. Here, $C_l = 3$, $C_T = 1$, and $C_t = 9$, implying that one day running of the model test represents nine days for the prototype.

2.3. Test Procedure. The model test system includes a test chamber, a controlling system for both temperature and air circulation, and a data acquisition system. The test chamber is sized at 6000 mm × 5000 mm × 4000 mm, and the ambient temperature was live adjusted by using the temperature controlling device with a range of −40–65°C and an accuracy

Table 1: Meteorological data for the Jinghui Irrigation Area.

Meteorological factor	Data
Annual mean precipitation (mm)	538.9
Annual evaporation (mm)	1212
Annual average sunshine hours (h)	2200
Annual highest phreatic water level in winter (m)	3.0
Annual average freezing index (°C·d)	77
Lowest daily average temperature (°C)	−13.6
Annual average temperature (°C)	13.4
Annual average frozen depth (cm)	20–40
Frost-free period (d)	232

Table 2: Physical indexes for the taken loess.

Physical indexes	Data
Specific gravity, G_s	2.69
Dry density, ρ_d (g/cm^3)	1.50
Natural water content, w (%)	27.0
Atterberg limit	
Liquid limit, w_L (%)	33.9
Plastic limit, w_p (%)	18.7
Particle grading characteristics (%)	
0.075–2.0 mm	10.4
0.005–0.075 mm	65.3
<0.005 mm	24.3

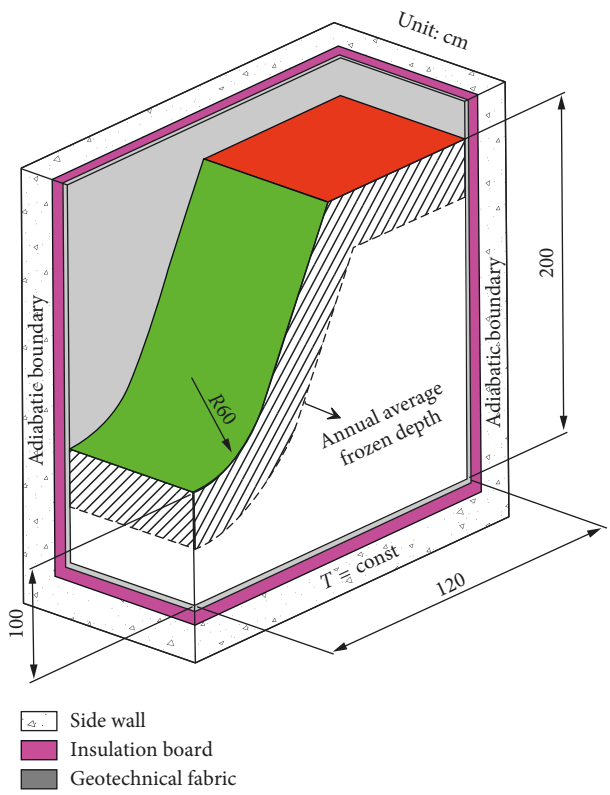

Figure 2: Schematic diagram for the U-shaped irrigation canal.

of ±0.2°C while the effective range for the bottom board is −25–65°C, with an accuracy of ±0.2°C. The air circulation system includes three main components: a cooling fan, a wind speed control device, and a ventilating duct. The data acquisition system is connected with four types of transducers, i.e., temperature, water content, deformation, and earth pressure, and the above four kinds of test data were live monitored. Based on the meteorological data in adjacent stations, the freezing period primarily includes three months for the selected irrigation area, i.e., Dec., Jan., and Feb. The thermal boundary applied on the top of the model can be determined in view of the monthly average temperatures, i.e., −9.5°C (0–80 h), −5.6°C (80–160 h), and −7.2°C (160–240 h). The freezing index was calculated based on the above three types of data, equal to 74.95°C·d, which is quite close to the measured data of 77°C·d, implying a rational thermal boundary in the model test.

Temperature transducers were produced by the platinum resistor with the range from −60 to 80°C and precision of ±0.01°C. The water content was live measured by the MYT-S102 transducer, with the range from 0 to 100% and precision of ±1%. Five typical monitoring points were set in the irrigation canal lining to monitor the frost heave performance of foundation soils, and the specific layout of the transducers is illustrated in Figures 3(a) and 3(b). The transducers for heat and water monitoring are placed beneath the surface of the canal bank that is demonstrated in red in Figure 2. The specific layout for the transducers is shown in Figure 3(c). The normal displacement of canal lining was measured by differential displacement sensors, and three key positions are focused, i.e., opening, slope, and bottom of the lining structure. The range and precision of the sensors are 0–10 cm and ±0.01 mm, respectively. The layered settlement-monitoring device was set in soils, and the preset induction metal ring can obtain the displacement of each layer, at an interval of 20 cm from the ground surface downward. The earth pressure cells were set in the interface between lining structure and soils, with the range from 0 to 4.0 MPa and precision of ±0.05%.

2.4. Results and Analysis

2.4.1. Water and Heat Migration during Freezing. The rate of cooling is influenced by many factors including speed and direction of wind, and underlying surface in that the air-cooling mode is employed during freezing of the model. Taking the left half of the canal model as an example, the monitored temperatures in the lining structure are selected to justify whether the minus-temperature boundary was effectively applied on the top of the model, as presented in Figure 4. Clearly, it demonstrates a relatively uniform thermal boundary at three characteristic time points as a whole, even though a particular temperature controlling mode of air-cooling is utilized in testing. The maximum difference among all the five monitoring points is 0.15°C, lower than the predefined precision in temperature control during the model test, i.e., ±0.2°C, indicating that this mode can well meet the requirements of temperature controlling.

As for the irrigation canal, the time history of ground temperatures in monitoring points is plotted in Figure 5. Obviously three stages can be noted from the development of the thermal regime for the canal foundation at the specified thermal boundary conditions. This is in accordance with the three levels of controlled temperatures in that a rapid cooling of the model occurs initially with the isothermal line of zero centigrade moving downward approximately linearly, as presented in Figure 5(a). The frozen depth of the canal foundation beneath the five characteristic points is presented in Figure 5(b). The isothermal lines for the frozen depth in the canal foundation shows similar distribution feature along the lining structure in that a particular temperature boundary is applied. Moreover, the cooling rate of the canal foundation can be considered as a result of the overlapping effect of both thermal boundaries in two primary directions such as the top of the canal and the large free surface that is intrinsically included in the canal lining. Thus, a faster cooling process at the opening of the canal foundation with lining structure is presented, and a higher rate of temperature change is produced within this range.

To verify the reliability of the transducers for water content, the stratified sampling was carried out in the canal bank of the model and the water content for each layer measured by the over-drying method is compared in Figure 6, together with the monitoring data by the transducers. The monitored water contents along with the depth agree well with the measured data by using the oven-drying

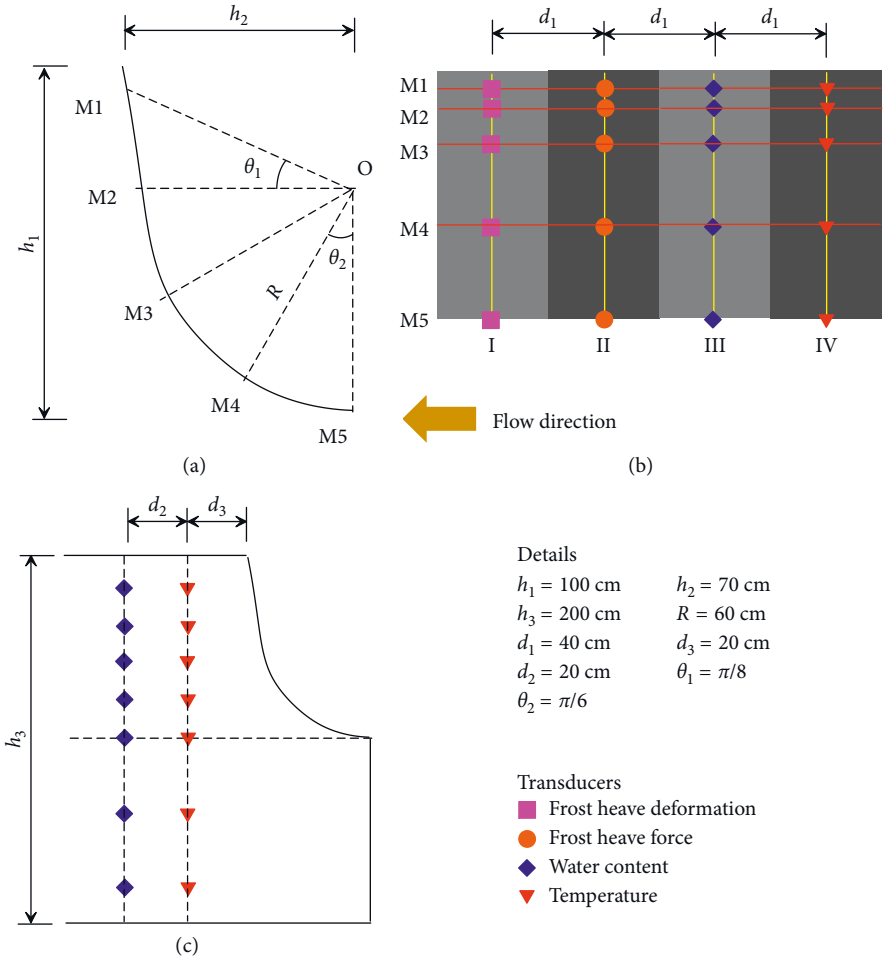

Figure 3: Specific layout of the transducers in the canal. (a) Five monitoring points in the lining structure. (b) Plan view. (c) Monitoring points in the canal bank.

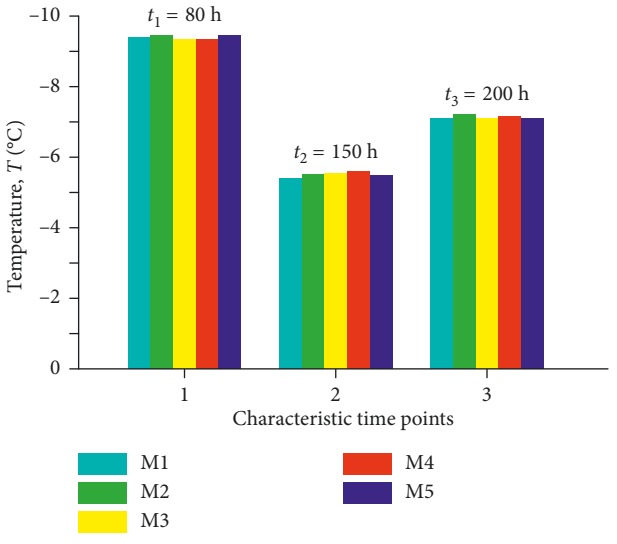

Figure 4: Comparison of temperatures in five monitoring points.

method, and this benefits from the merits that the dielectric constant is rarely affected by soil type, density, temperature, and hydraulic conductivity of pore water; thus no further calibration is required in testing [19]. Thus, the water content of the foundation soils monitored by the transducers is reliable in general.

Figure 7 illustrates the time history of the water content within certain depths of the canal foundation with no lining structure set above. The water content for canal bank exhibits complex variations at each layer and considerable migration of water can be easily noticed in surface layers with depth not deeper than 40 cm. This coincides well with the variation of ground temperature, and in detail, the migration and accumulation of water at a given minus-temperature occurs, especially at top of the model where the ground is easily influenced by ambient temperatures in two directions. However, the water content decreases with depth within a specified domain of 0–40 cm, while for the bottom of the foundation without water supply, little change can be noted and can be generally considered as a storage reservoir for further water migration during the freezing process.

To further reveal the variation of water content of soils beneath the canal foundation, the water contents monitored by the transducers set at two depths of 20 and 40 cm are plotted in Figure 8. As noted from the figure, the water

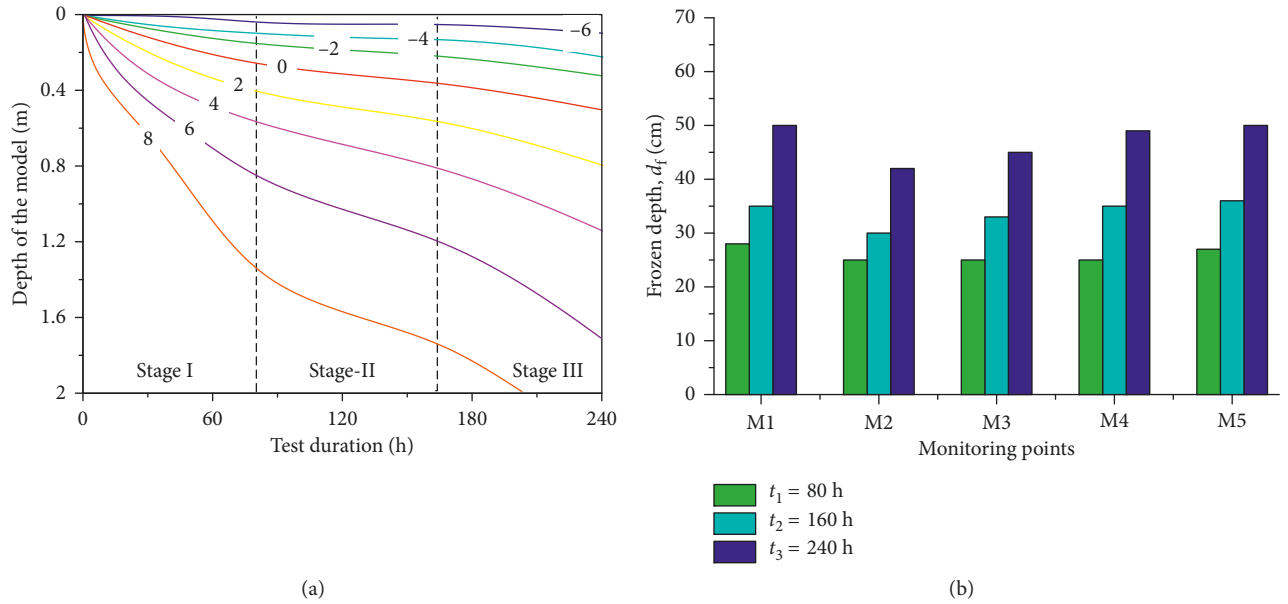

Figure 5: Thermal regime of the irrigation canal. (a) Time history for soils in the canal bank. (b) Frozen depth beneath the canal lining.

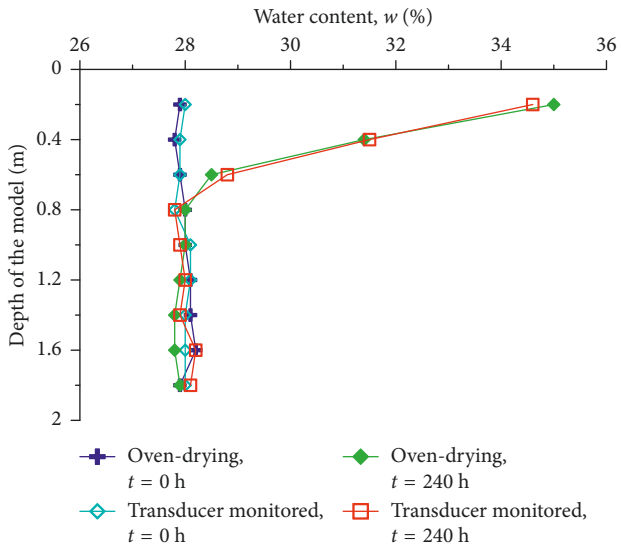

Figure 6: Comparison of water contents obtained by the transducer and oven-drying.

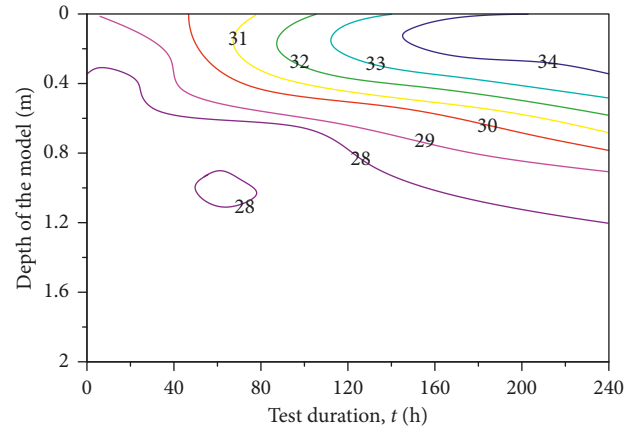

Figure 7: Time history of the water content in soils.

contents for foundation soils at the five characteristic points M1–M5 show similar variations to those at soil layers in the canal bank. Specifically, higher water contents can be found at a certain depth close to the opening of the irrigation canal, with a peak value existing at the opening. This results from the minus-temperature boundaries in two directions such as the top of the model and the upper part of the lining. Despite the overlapping effect in ground temperature, the water content also demonstrates a similar phenomenon. More accumulated water exists just beneath the lining, and it can be inferred that the accumulation of both heat and water may induce larger normal displacement in the canal lining and also the normal frost heave force was generated during freezing.

2.4.2. Frost Heave in Concrete Canal Lining. The fracture of canal lining primarily results from the frost heave of foundation soils that exerts on the concrete lining, and even more serious is the stress concentration generated during freezing; failure of materials occurs as the stress exceeds the tensile strength [31]. Figure 9 illustrates the normal deformation and force in the concrete lining due to frost heave. Both the normal deformation and force show obvious difference among five monitoring points. Even so, larger deformation and frost force are generated in both opening and bottom of the lining structure while the valley value exists at the intersection point between the tangential and arc segments, implying a more considerable stress release that leads to stress transfer towards the two endpoints. Meanwhile, the frost heave-induced deformation is lower and generally grows over test duration while the normal force due to frost heave tends to stabilize.

Here, a new index of K_f representing the uneven frost heave in the concrete canal lining is introduced among all considered monitoring points:

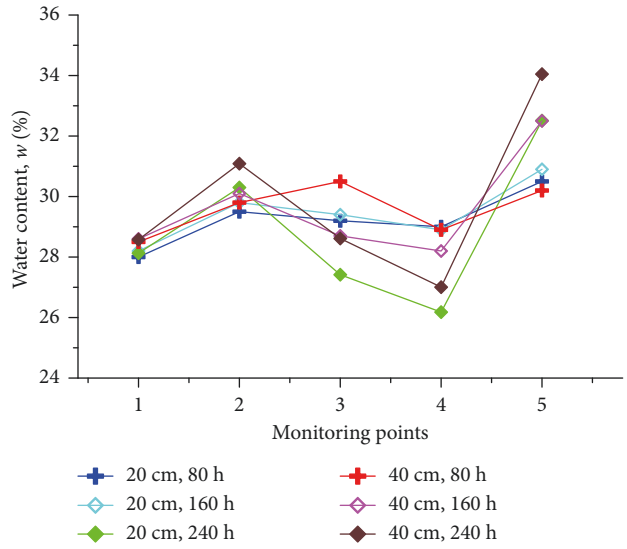

Figure 8: Water distribution in the canal foundation before and after testing.

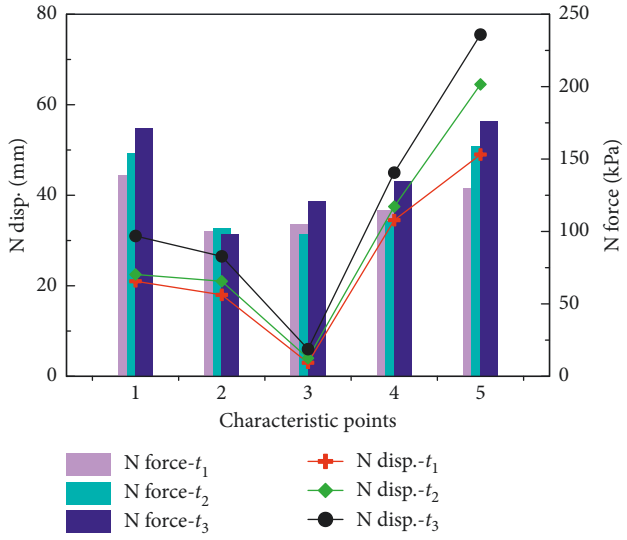

Figure 9: Normal deformation and force due to frost heave.

$$K_f = \frac{S_{max} - S_{min}}{S_{mean}}, \quad (2)$$

where S_{max}, S_{min}, and S_{mean} are the maximum, minimum, and mean gradient of frost actions to the relative distance. This can be directly determined from the measured characteristic variables:

$$S = \left| \frac{\delta_i - \delta_{i-1}}{x_i - x_{i-1}} \right|, \quad (3)$$

where δ is the measured characteristic indexes during frost heave including deformation, force, temperature, and water content and x is the relative distance between the two points, i.e., i and $i-1$. From the above equation, more uniform frost actions will be reached in the concrete canal lining as the value of K_f approaches to zero. In this case, little effect of frost heave on the concrete lining will be observed while the concentration of frost actions occurs at a higher value of K_f, e.g., the concentration of stress, and larger damage may be caused in the lining.

Substitute the four characteristic indexes into the above equations, and the index of nonuniform frost heave at three time points is calculated and presented in Figure 10. The indexes calculated corresponding to the three variables such as temperature, water content, and normal displacement decrease with elapsed time and within the first cooling stage, i.e., the lower temperature boundary; all the three variables due to frost heave of soils show a larger value of the nonuniform frost heave index. While for the normal force generated, a peak value is noted at time t_2, which may be related to the uneven gradient of frost actions to the relative distance. The geometric character may account for this trend. The deformation of the concrete lining consumes part of the energy generated during frost heave, and also the stress transfer occurs from the point where the stress is concentrated. These two processes may account for the decrease of the nonuniform frost heave index. Moreover, the thermal state characterized by the ground temperature is easily influenced by the geometry of the lining structure, and the evolution of thermal regime will be affected at given particular thermal boundaries. In addition, the index correlated with the water content varies within a narrow range. It can be inferred that obvious accumulation of soil water exists just beneath the lining structure, and experimental evidences can be found from the accumulated water in the weak drainage boundary of the foundation [32].

A recent literature by Li et al. [4] proves that the creep of foundation soils should also be included in estimating the total deformation during freezing period and introduces an empirical viscoplastic criterion to model the creep strain rate. It can be inferred that, at a certain depth of the irrigation canals, e.g., the normal flow depth in irrigation period, only the gravitational force of canal and flow water should be considered in predicting settlement of foundations. However, the creep of soils under self-weight accounts for a small proportion of the total and can be neglected for the sake of simplicity in practical engineering. Here, to verify the above point, the layered settlement of the canal foundation at various depths is illustrated in Figure 11. For foundation loess used in the model test, considerable frost heave-induced deformation occurred within the depth of 60 cm at a specific condition when the ground freezes after the autumn irrigation. However, deep soils exhibit lower deformation compared with the surface layers, and it should not be taken into account in practical engineering. However, one point to be concerned is that the migration of water towards the freezing front has always been in progress, and as a result, abundant liquid water supplies the necessitated amount during frost heave. In this case, the possible consolidation of saturated loess in the foundation might exist with the water discharged under gravity, and evidence can be

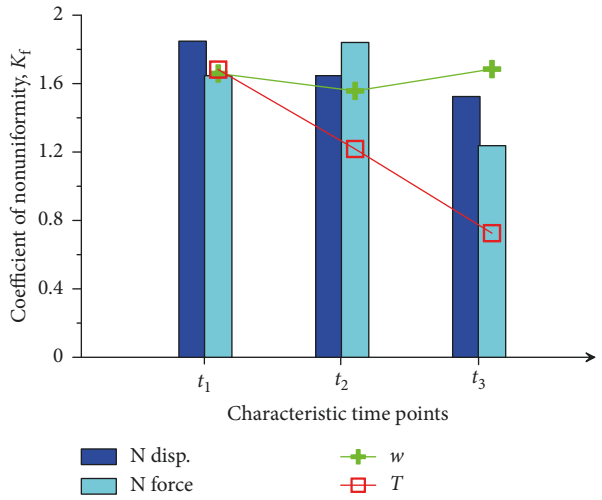

Figure 10: Nonuniform frost heave index at three durations.

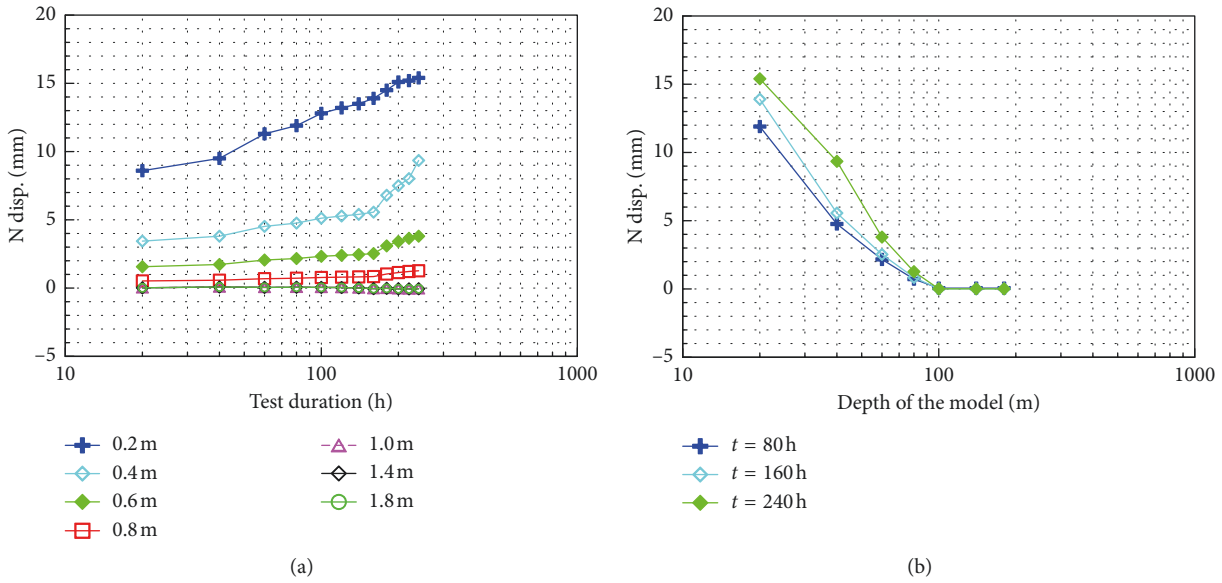

Figure 11: Layered deformation of foundation. (a) N disp. over time. (b) N disp. over the depth of the model.

noticed from the variation of water content along with the depth of the model. Correspondingly, the thermal regime shows little change.

Previous work proves that soil deforms over time and is primarily characterized by both consolidation and creep of soils. The former results from the compression of soil skeleton under effective stress and dissipation of excess pore water pressure while creep is a time-dependent deformation under a constant load. The mechanism for the two types of deformation is similar, but the stress state varies [33]. It is thus hard to separate the two processes, but the creep noticed from the model test only accounts for a negligible percentage of the total. Similar conclusions are drawn by Berre and Iversen [34] that a soft normally consolidated clay exhibits large secondary compression.

3. Modeling of Frost Heave of Irrigation Canals

3.1. Governing Equations

3.1.1. Heat Transfer Incorporating Ice-Water Phase Change. Provided that both convection and radiation are neglected in modeling soil freezing, the heat transfer considering ice-water phase change can be described as [35, 36]

$$-h_{i'i} + h_v = \rho C \frac{\partial T}{\partial t}, \tag{4}$$

with

$$h_i = -\lambda T_{i'}. \tag{5}$$

The phase change is assumed to occur within the temperature domain of $[T_b, T_f]$, and the "apparent" thermal

indexes listed below can be used including the equivalent specific heat C^* and equivalent heat conductivity λ^*:

$$C^* = C_f + \frac{C_u - C_f}{T_f - T_b}(T - T_b) + \frac{L}{1 + \theta_w}\frac{\partial \theta_i}{\partial T},$$
$$\lambda^* = \lambda_f + \frac{\lambda_u - \lambda_f}{T_f - T_b}(T - T_b), \quad (6)$$

where h_v is the heat source of fluid; the subscripts u and f denote soils in unfrozen and frozen states; L is the latent heat due to ice-water phase change; and θ_w and θ_i are the volumetric contents of water and ice, respectively. This method has been successfully used in engineering design of lifeline projects in Qinghai–Tibetan plateau such as bridges, highways, and irrigation canals [4, 37–39].

3.1.2. Water Migration in Freezing Soils. The vapor and ice flow are not considered here, and a modified Richards' equation for steady or unsteady fluid flow in a saturated or partially saturated soil during freezing can be described as [40]

$$\frac{\partial \theta_w}{\partial t} = \frac{\partial}{\partial z}\left[k(h)\frac{\partial h}{\partial z} + k(h) + k(h)\gamma h\frac{\partial T}{\partial z}\right], \quad (7)$$

where θ_w is the equivalent content of liquid water; z is the spatial coordinate; γ is the surface tension of soil water; and h is the water pressure head that can be determined from water retention curves for unfrozen soils, while for the frozen domain it is generally estimated by the generalized Clausius–Clapeyron equation. The ice pressure is assumed zero for the sake of simplicity [41]:

$$\frac{dP}{dT} = \frac{L_f}{v_w T}, \quad (8)$$

where P is the pressure ($P = \rho_w g h$), with g as the acceleration of gravity; L_f is the latent heat during soil freezing; and v_l is the specific volume of water.

The hydraulic conductivity for partially saturated frozen soils can be written as [40]

$$k(h) = -\frac{J_w}{(\Delta T/\Delta z)\gamma h + (\Delta h/\Delta z) + 1}, \quad (9)$$

where J_w denotes the water flux obtained from the derivative of equivalent water content θ_w with respect to time t. The equivalent water content θ_w can be deduced as

$$\theta_w = \theta_u + \frac{\rho_i}{\rho_w}\theta_i, \quad (10)$$

where $\theta_u = f(T)$ can be empirically determined by [12]

$$\theta_u = a_1 |T|^{-b_1}, \quad (11)$$

where a_1 and b_1 are experimental coefficients.

3.1.3. Establishment of the Frost Heave Model. The stress-strain relationship for frozen soils can be described as [4, 37]

$$\{\Delta\sigma\} = [D_T]\{\Delta\varepsilon_e\}, \quad (12)$$

with the elastic strain increment $\{\Delta\varepsilon_e\}$ determined by

$$\{\Delta\varepsilon_e\} = \{\Delta\varepsilon\} - \{\Delta\varepsilon_V\} - \{\Delta\varepsilon_P\}, \quad (13)$$

where $\{\Delta\varepsilon\}$ is the total strain increment; $\{\Delta\varepsilon_V\}$ is the strain increment due to frost heave; and $\{\Delta\varepsilon_P\}$ represents the plastic strain increment.

Frost heave characterizes the volumetric deformation of soils during freezing and primarily results from both phase transition from water to ice and pore water freezing in situ. The frost heave strain of soils in the "warm" frozen domain is given as [37]

$$\varepsilon_V = 1.09(\theta_0 + \Delta\theta_w - \theta_u) + \theta_u - n, \quad (14)$$

where θ_0 is the initial water content; $\Delta\theta_w$ is the increment of migrating water; and n denotes the porosity of soils.

Both frozen and unfrozen soils are considered to be isotropic, and the expansion strain in each direction is assumed to be equal [37]. Hence, $\{\Delta\varepsilon_V\}$ at the plane strain condition could be expressed as

$$\{\varepsilon_V\} = \frac{1}{3}\varepsilon_V\{1 + \nu_T \quad 1 + \nu_T \quad 0\}^T. \quad (15)$$

Compression of clayey soils in both thawed state and "cold" frozen domain is calculated based on the Drucker–Prager yield criterion:

$$\alpha I_1 + \sqrt{J_2} = k_1, \quad (16)$$

with

$$\alpha_1 = \frac{2\sin\phi}{\sqrt{3}(3 - \sin\phi)},$$
$$k_1 = \frac{6c\cos\phi}{\sqrt{3}(3 - \sin\phi)}, \quad (17)$$

where the parameters c and ϕ are the cohesion and angle of internal friction. Note that the "warm" and "cold" frozen soils are classified based on a temperature limit suggested by Qi and Zhang [38], i.e., −1.0°C.

3.2. Geometric Model and Definite Conditions. The shady half of the selected section is taken in numerical modeling for the sake of safety in which the slope orientation may cause considerable imbalance of heat absorption in both sides as the canal runs from west to east. The geometric model with sizes identical to the in situ is employed here, as presented in Figure 12. The highest underground water table of about 3.0 m is obtained from several years' observation, and a conservative value of h_1, equal to 10.0 m, is taken as the depth of the model while the depth labeled as h_2 is 7.0 m considering both depth of flow and normal canal freeboard. The thickness of the insulation board d_2 is taken to be 1/10–1/15 of the frozen depth. Both sides of the geometric model are assumed as adiabatic boundaries, where the fixed nodal temperatures are applied. A simplified constant thermal boundary is specified at the bottom, and a mean value of 16.5°C is exerted that was noted from the monitored ground temperature in adjacent meteorological stations

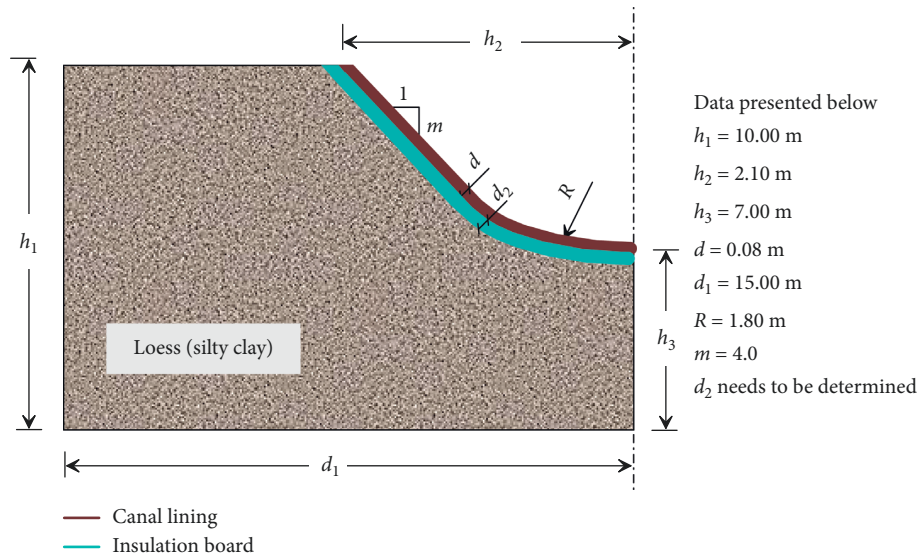

Figure 12: Geometric model for numerical computation.

[42], which is independent of the atmospheric circulation. The monthly average temperature in the freezing period is given as the upper temperature boundary. The x-scale nodal displacement is fixed in both sides, while free y-scale displacements are specified for nodes. The in situ measured profiles of ground temperature and water content are taken as the initial conditions for computation, as presented in Figure 13.

3.3. Determination of Model Parameters. Both canal lining and joint sealing materials were assumed elastic, and the mechanical parameters are obtained from the literature [30, 31], as listed in Table 3. However, the loess used as the foundation of the irrigation canal is assumed as elastoplastic, and its response to the surcharge load can be described by the Drucker–Prager yield criterion. The mechanical parameters used in computation are obtained based on the test data presented in the literature [43]. Following the work by Li et al. [4], the empirical equation below is used in describing the mechanical behaviors of frozen soils at various temperatures:

$$Y_i = a_i + b_i|T|^m, \tag{18}$$

where the subscript i (i = 1 – 4) represents the elastic modulus, Poisson's ratio, cohesion and angle of internal friction, respectively. The parameter m can be taken as 0.6 for the elastic modulus of frozen clayey soils while m is equal to 1.0 for the other three [19]. The parameters of b_i (i = 1 – 4) are equal to zero for thawed soils, while for frozen soils, the parameters are obtained by the test. The characteristic parameters for heat and water migration in loess are listed in Table 4. Here, the hydraulic conductivity for loess is measured at a reference temperature of 20°C, while for soils at various temperatures, it can be adjusted based on the varying viscosity with respect to temperature [44]. The basic parameters for the EPS insulation board are listed in Table 5.

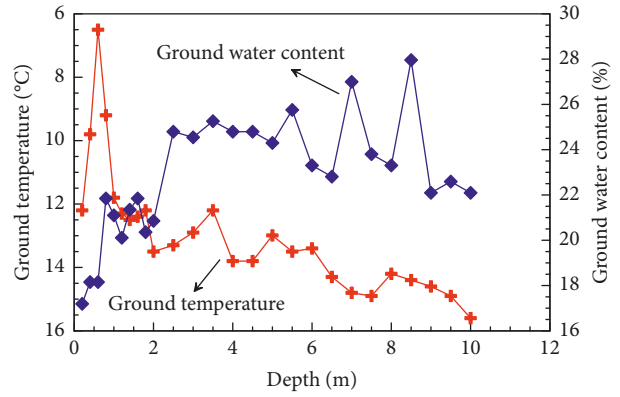

Figure 13: In situ measured ground water content and temperature.

Table 3: Mechanical properties of materials in canal.

Type of materials	Parameters	Data
Concrete	E (GPa)	24
	V	0.167
	ρ (kg/m^3)	2500
Joint sealing materials	E (MPa)	0.20
	V	0.45
	ρ (kg/m^3)	1900
Foundation loess	a_1 (MPa)	0.57
	b_1 (MPa/°C)	0.55
	a_2	0.40
	b_2	−0.008
	a_3 (MPa)	0.15
	b_3 (MPa/°C)	0.055
	a_4 (°)	12
	b_4 (°/°C)	1.60

3.4. Comparison of Simulated and Measured Data. Figure 14 illustrates the comparison of the calculated frozen depth and water content versus the measured data to

Table 4: Characteristic indexes for heat and water migration for loess.

Indexes	Data
Specific heat, C (kJ/(kg·°C))	
Frozen state	1.67
Thawed state	1.38
Heat conductivity, λ (W/(m·°C))	
Frozen state	1.24
Thawed state	1.00
Permeability, K (10^{-7} m/s)	6.12
Unfrozen water, w_u	
a (%/°C)	17.67
b	0.70

Table 5: Physical indexes for the EPS insulation board.

Indexes	Data
Density, ρ (g/cm^3)	15–40
Water absorption (%)	<6.0
Dimensional stability (−40–70°C) (%)	<4.0
Thermal conductivity, λ (W/(m·°C))	<0.041
Compressive strength (kPa)	20–80

verify the rationality of the model. For cases when the concrete lining is not considered, the calculated thermal regime agrees well with the test data, especially at the opening of the irrigation canal lining where complex water and heat migration is noticed, e.g., the point M1. Besides, the water content calculated is slightly higher than that in computation. This may be related to the basic assumptions for numerical computation; that is, materials in the computational domain are assumed as the homogeneously isotropic medium, which differs from the actual state of the filling loess, i.e., the spatial variability. Even so, the five monitoring points all show similar variations in general, and the magnitude all approach to the measured data. Moreover, the computed normal frost heave force and normal displacement show good agreement with the measured, with lower indexes of nonuniform frost heave for the all considered points. This implies that the inhomogeneity of filling materials also leads to the deviation of mechanical responses due to frost heave, with the magnitude lower than 10%, proving that the practical model proposed here is reliable in predicting the frost heave of the irrigation canals filled by loess. Moreover, the computed normal frost heave force and normal displacement show good agreement with the measured ones, with lower indexes of nonuniform frost heave for all the considered points, as shown in Figure 15.

3.5. Thickness of Insulation Board Determined by the Partial Insulation Method. The thickness of the insulation board for small- and medium-sized canals is taken as 1/10–1/15 of the frozen depth, while for large-scale irrigation canals, this is determined based on thermal computations to completely eliminate the overall frost heave. In this case, the frozen depth is controlled as zero after the insulation board is set beneath the lining structure, which is called the overall insulation method. However, this engineering measure has not been

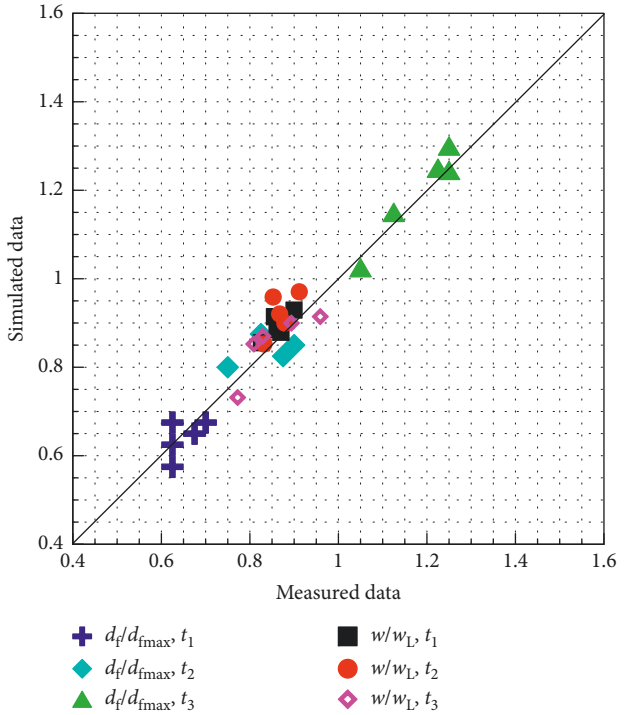

Figure 14: Comparison of calculated frozen depth and water content and measured data.

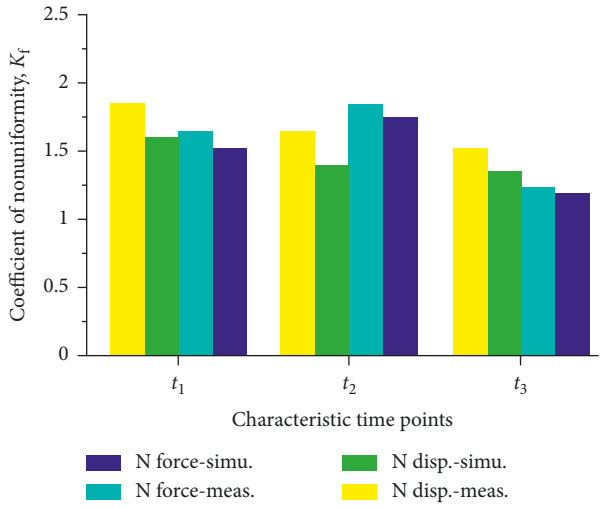

Figure 15: Comparison of calculated frost heave-induced deformation and force and monitored data.

widely used due to such a high construction cost in preserving the stability of the irrigation canal in the cold season. Thaw settlement of the irrigation canal occurs in spring, based on which An et al. [30, 31] suggest that the thickness could be reduced by utilizing the merit that a certain amount of frost heave could be recovered due to thawing settlement. Thus, an allowable frost heave is assumed to occur at a specified domain beneath the insulation board, where a fully saturated medium is reached, and this particular value is taken as the allowed normal displacement by fully utilizing the probable settlement due to thawing of seasonal frozen ground. Moreover, the insulation board also leads to the delay of the

freezing period, and the intensity of frost heave is weakened. Hence, this partial insulation method is more economic and rational in antifrost of the irrigation canals. Here, the thickness of the insulation board can be empirically determined, including three main parts, i.e., opening (M1-M2), slope surface (M2-M4), and bottom (M4-M5). For the sake of safety, the thickness for each parts can be taken as 1/10 of the froze depth, i.e., 5.1, 4.5, and 4.9 cm. A new geometric model is established based on the above three thicknesses, and the normal deformation and force due to frost heave will be calculated and compared with the data obtained as no insulation board is set, as presented in Figure 16. Clearly as it shows, more than 80% of the maximum frost heave deformation will be cut down with the EPS insulation board and the newly calculated normal deformation is 1.05 cm, lower than the allowed value of 2.0 cm, indicating that it is applicable by using the EPS insulation board.

However, this kind of antifrost performance is based on a relatively thicker insulation board, and a moderate decrease in the thickness could be used as an alternative by assuming that the allowed normal deformation of 2.0 cm can be reached. Thus, the thickness of the insulation board for the three positions can be successively scaled down by 0.9, and the normal deformation and force due to frost heave can be calculated by iterating through the three positions. The specific size for the insulation board after trials is listed in Table 6. From the table, the original size for the insulation board is about 5.0 cm, and a good antifrost effect can be obtained but is not an optimal solution. Based on the partial insulation method, a certain amount of frost heave deformation is allowed in frozen depth to balance the potential thaw settlement in spring. The trial results prove that the thickness will be cut down about 1.0–1.4 cm, and the material expense per unit length is 0.048 m^3, with the cost saving per unit length of 11.6 RMB. Thus, an economic measure can be used in preventing the frost heave of irrigation canals.

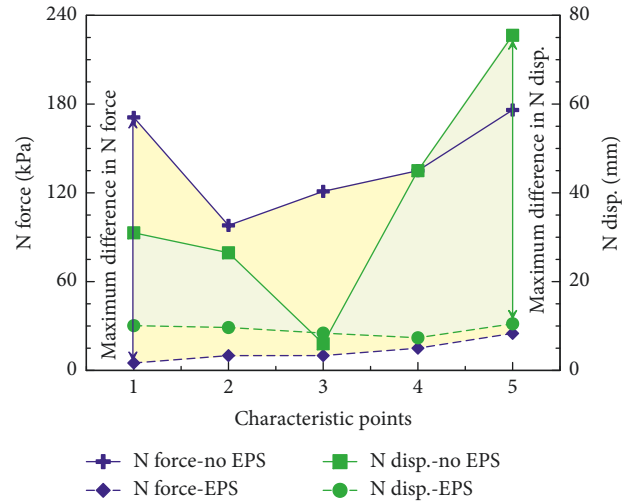

Figure 16: Antifrost effect of the insulation board.

Table 6: Physical indexes for the EPS insulation board.

Method	Thickness of insulation board (cm)			Material expense per unit length (m^3)	Cost per unit length (RMB)
	Opening	Slope	Bottom		
Overall insulation	5.1	4.5	4.9	0.194	46.6
Partial insulation	3.7	3.5	3.6	0.146	35.0

4. Conclusions

This paper investigates the frost heave behaviors of a U-shaped irrigation canal including coupled heat and water migration, development of the frost heave-induced normal deformation, and normal force in the canal lining structure; especially the frost heave occurs at a specified frozen depth. The index of nonuniform frost heave shows that both opening and bottom of the lining structure exhibit larger deformation and frost heave force during freezing when a predefined thermal boundary is applied. The layered deformation monitored indicates that creep of underlying soils accounts for a negligible proportion of the total deformation and can be neglected in practical engineering for the sake of simplicity. Only the frost heave should be taken into account when analyzing the frost actions at given thermal boundaries.

A practical model incorporating both modified Richards' equation and heat transfer equation with ice-water phase change is proposed based on the assumption that frost heave of soils originates from the phase transition of both migrated and original water into ice and in situ water into ice. The above model test is simulated and the rationality of the proposed model is verified. Based on the partial insulation method, the thickness of the insulation board is calculated. Results indicate that, for three typical positions of the canal lining, i.e., opening, slope surface, and bottom of the canal, the reasonable thicknesses of the insulation board are 3.7, 3.5, and 3.6 cm, respectively, and better antifrost effect can be obtained with lower economic input.

Data Availability

The data used to support the findings of this study are available from the corresponding author upon request.

Conflicts of Interest

The authors declare no conflicts of interest.

Acknowledgments

This research was financially supported by the National Natural Science Foundation of China (Nos. 51478385, 51778528, 51878551, and 51574219). These supports are greatly appreciated.

References

[1] W. Gu, D. Shao, and Y. Jiang, "Risk evaluation of water shortage in source area of middle route project for South-to-North water transfer in China," *Water Resources Management*, vol. 26, no. 12, pp. 3479–3493, 2012.

[2] Q. Huang, "Impact evaluation of the irrigation management reform in northern China," *Water Resources Research*, vol. 50, no. 5, pp. 4323–4340, 2014.
[3] P. C. Li, "New problems and mission of agricultural water and soil engineering in China," *Journal of Shenyang Agricultural University*, vol. 35, no. 5-6, pp. 373–377, 2004, in Chinese.
[4] S. Li, M. Zhang, Y. Tian, W. Pei, and H. Zhong, "Experimental and numerical investigations on frost damage mechanism of a canal in cold regions," *Cold Regions Science and Technology*, vol. 116, pp. 1–11, 2015.
[5] Q. Zhu, "Frost heave prevention measures for canal linings in China," *Irrigation and Drainage Systems*, vol. 5, no. 4, pp. 293–306, 1991.
[6] T. F. Azmatch, D. C. Sego, L. U. Arenson, and K. W. Biggar, "New ice lens initiation condition for frost heave in fine-grained soils," *Cold Regions Science and Technology*, vol. 82, pp. 8–13, 2012.
[7] H. Guan, D. Wang, W. Ma et al., "Study on the freezing characteristics of silty clay under high loading conditions," *Cold Regions Science and Technology*, vol. 110, pp. 26–31, 2015.
[8] Y. Lai, W. Pei, M. Zhang, and J. Zhou, "Study on theory model of hydro-thermal-mechanical interaction process in saturated freezing silty soil," *International Journal of Heat and Mass Transfer*, vol. 78, pp. 805–819, 2014.
[9] W. Ma, L. Zhang, and C. Yang, "Discussion of the applicability of the generalized Clausius-Clapeyron equation and the frozen fringe process," *Earth-Science Reviews*, vol. 142, pp. 47–59, 2015.
[10] B. Liu and D. Li, "A simple test method to measure unfrozen water content in clay-water systems," *Cold Regions Science and Technology*, vol. 78, pp. 97–106, 2012.
[11] J. G. Dash, "Thermomolecular pressure in surface melting: motivation for frost heave," *Science*, vol. 246, no. 4937, pp. 1591–1593, 1989.
[12] X. Z. Xu, J. C. Wang, and L. X. Zhang, *Physics of Frozen Soils*, Science Press, Beijing, China, 2001, in Chinese.
[13] V. E. Romanovsky and T. E. Osterkamp, "Effects of unfrozen water on heat and mass transport processes in the active layer and permafrost," *Permafrost and Periglacial Processes*, vol. 11, no. 3, pp. 219–239, 2015.
[14] H. Bing and P. He, "Frost heave and dry density changes during cyclic freeze-thaw of a silty clay," *Permafrost and Periglacial Processes*, vol. 20, no. 1, pp. 65–70, 2009.
[15] Y.-Z. Zou and C. Boley, "Compressibility of fine-grained soils subjected to closed-system freezing and thaw consolidation," *Mining Science and Technology (China)*, vol. 19, no. 5, pp. 631–635, 2009.
[16] X. Zhang, M. Zhang, W. Pei, and J. Lu, "Experimental study of the hydro-thermal characteristics and frost heave behavior of a saturated silt within a closed freezing system," *Applied Thermal Engineering*, vol. 129, pp. 1447–1454, 2018.
[17] S. Akagawa, "Experimental study of frozen fringe characteristics," *Cold Regions Science and Technology*, vol. 15, no. 3, pp. 209–223, 1988.
[18] K. Watanabe, M. Mizoguchi, T. Ishizaki, and M. Fukuda, "Experimental study on microstructure near freezing front during soil freezing," in *Proceedings of the International Symposium on Ground Freezing and Frost Action in Soils*, pp. 187–192, Lulea, Sweden, April 1997.
[19] Y. M. Lai, M. Y. Zhang, and S. Y. Li, *Engineering Theory and Application in Cold Regions Engineering*, Science Press, Beijing, China, 2009, in Chinese.
[20] P. B. Black and R. D. Miller, "Hydraulic conductivity and unfrozen water content of air-free frozen silt," *Water Resources Research*, vol. 26, no. 2, pp. 323–329, 2010.
[21] K. Horiguchi and R. D. Miller, "Hydraulic conductivity functions of frozen materials," in *Proceedings of 11th International Conference on Permafrost*, pp. 503–508, National Academy Press, Washington, DC, USA, 1983.
[22] T. P. Burt and P. J. Williams, "Hydraulic conductivity in frozen soils," *Earth Surface Processes*, vol. 1, no. 4, pp. 349–360, 1976.
[23] J. F. Nixon, "Discrete ice lens theory for frost heave in soils," *Canadian Geotechnical Journal*, vol. 28, no. 6, pp. 843–859, 1991.
[24] J.-M. Konrad, "Sixteenth Canadian Geotechnical Colloquium: frost heave in soils: concepts and engineering," *Canadian Geotechnical Journal*, vol. 31, no. 2, pp. 223–245, 1994.
[25] R. W. Style and S. S. L. Peppin, "The kinetics of ice-lens growth in porous media," *Journal of Fluid Mechanics*, vol. 692, no. 2, pp. 482–498, 2012.
[26] P. B. Black, "RIGIDICE model of secondary frost heave," CRREL Report 95-12, Cold Regions Research and Engineering Laboratory, Hanover, NH, USA, 1995.
[27] H. Zheng, S. Kanie, F. Niu, and A. Li, "Three-dimensional frost heave evaluation based on practical Takashi's equation," *Cold Regions Science and Technology*, vol. 118, pp. 30–37, 2015.
[28] N. Li, F. Chen, B. Xu, and G. Swoboda, "Theoretical modeling framework for an unsaturated freezing soil," *Cold Regions Science and Technology*, vol. 54, no. 1, pp. 19–35, 2007.
[29] Y. Zhou and G. Zhou, "Intermittent freezing mode to reduce frost heave in freezing soils—experiments and mechanism analysis," *Canadian Geotechnical Journal*, vol. 49, no. 6, pp. 686–693, 2012.
[30] P. An, Y. C. Xing, and A. J. Zhang, "Thickness calculation and numerical simulation of insulation board for canal using partial insulation method," *Transactions of the Chinese Society of Agricultural Engineering*, vol. 29, no. 17, pp. 54–62, 2013, in Chinese.
[31] P. An, Y. C. Xing, A. J. Zhang, and P. T. Zhu, "Study of design method and numerical simulation for anti-frost heave cushion of canal," *Rock and Soil Mechanics*, vol. 34, no. s2, pp. 257–264, 2013, in Chinese.
[32] Z. Q. Zhang, Q. B. Wu, Z. Wen, Y. Z. Liu, and Z. J. Lu, "Analysis of moisture accumulation process on frozen soil subgrade of asphalt pavement," *China Journal of Highway and Transport*, vol. 26, no. 2, pp. 1–6, 2013.
[33] H. H. Zhu, X. P. Chen, X. J. Cheng, and B. Zhang, "Study on creep characteristics and model of soft soil considering drainage condition," *Rock and Soil Mechanics*, vol. 27, no. 5, pp. 694–698, 2006, in Chinese.
[34] T. Berre and K. Iversen, "Oedometer test with different specimen heights on a clay exhibiting large secondary compression," *Géotechnique*, vol. 22, no. 1, pp. 53–70, 1972.
[35] X. Yao, J. Qi, and W. Wu, "Three dimensional analysis of large strain thaw consolidation in permafrost," *Acta Geotechnica*, vol. 7, no. 3, pp. 193–202, 2012.
[36] X. Yao, J. Qi, M. Liu, and F. Yu, "Pore water pressure distribution and dissipation during thaw consolidation," *Transport in Porous Media*, vol. 116, no. 2, pp. 435–451, 2016.
[37] Y. Lai, X. Zhang, J. Xiao, S. Zhang, and Z. Liu, "Nonlinear analyses for frost-heaving force of land bridges on Qinghai-Tibet Railway in cold regions," *Journal of Thermal Stresses*, vol. 28, no. 3, pp. 317–331, 2005.
[38] J. L. Qi and J. M. Zhang, "Definition of warm permafrost based on mechanical properties of frozen soils," in *Proceedings of 9th International Conference on Permafrost*, pp. 1457–1461, Fairbanks, AK, USA, June-July 2008.

[39] F. Yu, M. Zhang, Y. Lai, Y. Liu, J. Qi, and X. Yao, "Crack formation of a highway embankment installed with two-phase closed thermosyphons in permafrost regions: field experiment and geothermal modelling," *Applied Thermal Engineering*, vol. 115, pp. 670–681, 2017.

[40] K. Watanabe and T. Wake, "Hydraulic conductivity in frozen unsaturated soil," in *Proceedings of 9th International Conference on Permafrost*, pp. 147–152, Fairbanks, AK, USA, June-July 2008.

[41] K. Hansson, J. Šimůnek, M. Mizoguchi, L. C. Lundin, and M. T. V. Genuchten, "Water flow and heat transport in frozen soil," *Vadose Zone Journal*, vol. 3, no. 2, pp. 527–533, 2004.

[42] S. H. Li, Y. Wang, and H. X. Cao, "Anomalous features of geotemperature in the depth of 10 m by Gaoling observation point before the 1998 Jingyang Ms4.8 earthquake, Shaanxi Province," *Northwestern Seismological Journal*, vol. 23, no. 2, pp. 117–119, 2001, in Chinese.

[43] W. Ma and D. Y. Wang, *Frozen Soil Mechanics*, Science Press, Beijing, China, 2014, in Chinese.

[44] S. Wang, J. Qi, F. Yu, and F. Liu, "A novel modeling of settlement of foundations in permafrost regions," *Geomechanics and Engineering*, vol. 10, no. 2, pp. 225–245, 2016.